Journal of Power Sources 195 (2010) 4234–4241

Contents lists available at ScienceDirect

Journal of Power Sources

journal homepage: www.elsevier.com/locate/jpowsour

A new type of high energy asymmetric capacitor with nanoporous carbon electrodes in aqueous electrolyte

V. Khomenko, E. Raymundo-Piñero, F. Béguin*

Centre de Recherche sur la Matière Divisée, CNRS-University, 1B rue de la Férollerie, 45071 Orléans, France

ARTICLE INFO

Article history:
Received 11 October 2009
Received in revised form
19 December 2009
Accepted 3 January 2010
Available online 11 January 2010

Keywords:
Electrochemical capacitor
Aqueous electrolyte
Asymmetric configuration
High voltage
Activated carbon
Pseudo-faradaic reactions

ABSTRACT

A new type of low cost and high energy asymmetric capacitor based on only activated carbons for both electrodes has been developed in a safe and environment friendly aqueous electrolyte. In such electrolyte, the charges are stored in the electrical double-layer and through fast faradaic charge transfer processes. By taking profit of different redox reactions occurring in the positive and negative ranges of potential, it is possible to optimize the capacitor either by balancing the mass of the electrodes or by using different optimized carbons for the positive and negative electrodes. The best results are obtained in the latter case, by utilizing different pseudo-faradaic properties of carbons in order to increase the capacitance and to shift the potentials of water decomposition and destructive oxidation of activated carbon to more negative and positive values, respectively. After an additional adjustment of potentials by mass-balancing the two electrodes, the electrochemical capacitor can be reversibly charged/discharged at 1.6 V in aqueous medium, with energy densities close to the values obtained with electrical double-layer capacitors working in organic electrolytes, while avoiding their disadvantages.

1. Introduction

Electrochemical capacitors (or supercapacitors) are very attractive energy storage devices for a large number of applications. In most cases they are used to deliver a high power during a short time, being often associated to a battery, which in turn provides a high specific energy.

Since the amount of electrical energy (E) accumulated in such capacitors is given by the formula:

$$E = \frac{1}{2}CU^2 \quad (1)$$

where (C) is the capacitance and (U) is the voltage, the strategies for obtaining high performance devices depend on the optimization of these two parameters. The voltage depends on the stability window of the electrolyte. For aqueous electrolytes, the practical operating voltage is about 0.6–0.8 V while, in organic electrolytes, the electrochemical capacitor may operate at voltages between 2.5 V and 2.7 V. The capacitance depends essentially on the material and can arise from two different mechanisms: (i) an electrostatic attraction between charges along an electrical double-layer (EDL) formed at the electrode/electrolyte interface, which according to formula:

$$C_e = \frac{\varepsilon S}{d} \quad (2)$$

is controlled by the surface area S of the interface; and (ii) fast pseudo-faradaic charge transfer reactions between the electrode and the electrolyte [1,2]. Presently, the electrical double-layer capacitors (EDLC) using activated carbon electrodes in organic electrolyte are mostly available on the market. Taking into account formulae (1) and (2), the reasons of this choice are the high specific surface area of activated carbons and the high attainable voltage in organic electrolyte. However, in comparison with aqueous electrolytes, the organic electrolyte, e.g., tetraethylammonium tetrafluoroborate ($TEABF_4$) in acetonitrile, presents serious drawbacks: (i) a low conductivity which precludes the use of high charge and discharge currents, resulting in a limited power of the systems; (ii) a specific capacitance in the range of 50–150 F g^{-1} of activated carbon whereas values of 150–250 F g^{-1} can be obtained in aqueous electrolytes [3]; (iii) the need of building the systems in a moisture-free atmosphere, leading to a cost increase; and (iv) the environment unfriendly character of acetonitrile.

From the foregoing, it results clearly that electrochemical capacitors using aqueous electrolytes would be more attractive from an industrial point of view, but it is necessary to find strategies for increasing the amount of energy stored. On the basis of Eq. (1), this purpose can be achieved either by finding materials with enhanced capacitance or by increasing the working voltage window.

* Corresponding author.
E-mail address: beguin@cnrs-orleans.fr (F. Béguin).

0378-7753/$ – see front matter © 2010 Elsevier B.V. All rights reserved.
doi:10.1016/j.jpowsour.2010.01.006

1.1. Capacitance enhancement by pseudo-faradaic processes

The specific capacitance of materials displaying pseudo-faradaic charge transfer reactions, as metallic oxides [4–7] or conducting polymers [7–10], is higher than for typical EDL carbons. However they do not meet by far the criteria for an industrial application, e.g., low cost and high electrochemical stability. By contrast, nanoporous carbons might in some cases exhibit pseudo-capacitive properties and become very attractive electrode materials. The first case is when they contain heteroatom-based functional groups able to undergo pseudo-faradaic charge transfer reactions and hereto contribute together with the double-layer effect to the total capacitance of the material [11–14]. In this sense, some oxygen-rich and nitrogen-rich carbons with a relatively small specific surface area demonstrate capacitance values comparable to the best activated carbons available on the market [15–17]. The second possibility of pseudo-capacitive behavior of nanoporous carbons is observed when hydrogen is stored through negative polarization at potentials lower than the thermodynamic value for water reduction [18]. The reversible desorption of hydrogen generally occurs with a relatively important polarization, showing that hydrogen is weakly bonded to the surface of the carbon host [19]. Due to this state of hydrogen, the self-discharge is negligible, allowing this property to be applied for enhancing the capacitive properties of carbons.

1.2. Voltage enhancement by designing asymmetric capacitors

Hybrid or asymmetric configurations have been proposed for increasing the voltage of electrochemical capacitors in aqueous electrolytes [20–24]. In particular, it has been shown that a cell voltage around 2.0 V can be reached with an asymmetric configuration using environment friendly MnO_2 as positive electrode and activated carbon as negative one [22–24]. However, the capacitance value of the manganese oxide positive electrode is only 200–250 F g^{-1} that is far from the theoretical value, e.g., 1370 F g^{-1} [25]. Additionally, until now, non-optimized activated carbons were implemented at the negative electrode.

In this presentation, we introduce a new concept of asymmetric capacitor working in aqueous electrolyte, where the two electrodes are based on nanoporous carbon. The system takes profit of the different pseudo-faradaic reactions which occur in the positive and negative potential ranges and it is optimized either by balancing the mass of the electrodes or/and by using two different optimized carbons as positive and negative electrode. It demonstrates a higher capacitance than symmetric capacitors and it can operate up to 1.6 V in aqueous electrolyte.

2. Experimental

The activated carbons selected for the study were commercial samples from Norit (SUPER 50 – Carbon A) and Kansai (Maxsorb – Carbon B). Different chemical treatments have been performed to modify the surface functionality of the materials. The carbon A_{ox} was obtained by oxidizing the carbon A (1 g) with 20 mL of 30 wt% HNO_3 solution at 80 °C during 1 h. The oxidation of B in the same nitric acid medium had a deleterious effect on the porous texture which completely collapsed. Therefore, an oxidized carbon B_{ox} was obtained by mild oxidation of B (1 g) with 40 mL of 20 wt% H_2O_2 solution at room temperature during 1 h. After oxidation, the materials were extensively rinsed with distilled water.

The porous texture of the materials was analyzed by N_2 and CO_2 adsorption (Autosorb-1, Quantachrome) at 77 K and 273 K, respectively. The specific surface area, S_{BET}, was calculated from the N_2 adsorption isotherm by applying the BET equation. The micropore (<2 nm) and mesopore (2–50 nm) volumes have been extracted from the pore size distribution obtained by applying the DFT equation to the N_2 adsorption data. The CO_2 adsorption isotherms at 273 K and low relative pressure $P/P_0 < 0.1$ are assumed to correspond to the adsorption in narrow micropores from 0.4 nm to 0.8 nm (ultramicropores). They were used for the calculation of the ultramicropore volume according to the Dubinin–Radushkevich equation. Surface functionality was analyzed by X-ray photoelectron spectroscopy (XPS) on powders of the materials with a VG ESCALAB 250 spectrometer using an Al K_α monochromatic source (15 kV, 15 mA) and a multidetection analyzer, under 10^{-8} Pa residual pressure.

Electrodes were pressed from a mixture of activated carbon (85%), polyvinylidene fluoride PVDF (10%) and carbon black (Pure Black, Superior Graphite, 5%). Three different cell configurations have been used for realizing the electrochemical characterizations: (i) two-electrode capacitors were built in a teflon Swagelok® type system with a glassy fibrous separator and gold current collectors; the electrolytic solutions were 6 mol L^{-1} KOH and 1 mol L^{-1} H_2SO_4, respectively; (ii) the previous cell in which a reference electrode (Hg/HgO or Hg/Hg_2SO_4 in 6 mol L^{-1} KOH and 1 mol L^{-1} H_2SO_4, respectively) was added; and (iii) a classical three-electrode configuration using activated carbon as working electrode, Pt as counter electrode and a reference electrode. The gravimetric capacitance C expressed in Farad (F) per gram of carbon material was estimated by cyclic voltammetry at a scan rate of 2–100 mV s^{-1} and galvanostatic charge/discharge at a current density from 50 mA g^{-1} to 30 A g^{-1} using a VMP (Biologic, France) multi-channel generator. Impedance spectroscopy measurements were realized on the two-electrode capacitors using a VMP2 (Biologic, France). An ac amplitude of 20 mV was applied to reach the steady-state cell voltage, and the data were collected in the range of 100 kHz to 0.001 Hz.

3. Results and discussion

3.1. Physico-chemical characteristics of as-received and oxidized carbons

The data on porous texture and surface functionality of the various carbons are given in Table 1. The porous texture of both activated carbons A and B remains unchanged after their respective oxidation treatments (Table 1a). The carbons A and A_{ox} are essentially microporous, whereas carbons B and B_{ox} present a noticeable amount of mesopores together with micropores.

The surface functionality of as-received carbons A and B is quite comparable (Table 1b). After oxidation of A by nitric acid to give A_{ox}, the amount of surface oxygen increases from 4.6 at.% to 14.8 at.%. Actually, all kinds of oxygenated functionalities (carboxylic, quinone, phenolic and ether) increase after oxidation. By contrast, the oxidation treatment of B by H_2O_2 slightly enhances the total amount of oxygen from 5 at.% to 6.6 at.%, and in this case, only quinone and carboxylic functionalities are enriched.

3.2. Electrochemical characterization of carbons A and A_{ox}

Fig. 1 presents the cyclic voltammograms (CV) of three-electrode cells with A and A_{ox} in 1 mol L^{-1} H_2SO_4 or 6 mol L^{-1} KOH. In addition to the current due to charging/discharging the electrical double-layer, cathodic and anodic humps are observed at around −0.1 V vs Hg/Hg_2SO_4 and −0.5 V vs Hg/HgO in H_2SO_4 and KOH, respectively. The humps are more pronounced in the case of the oxidized sample, A_{ox}. For activated carbons, these peaks are traditionally assessed to redox reactions of oxygenated surface functionalities such as the quinone/hydroquinone (Q/HQ) pair or pyrone-like structures [13,26,27]. This interpretation fits well

Table 1
Physico-chemical characteristics of the as-received and oxidized activated carbons.

(a)Porous texture

Sample	S_{BET} (N_2) (m^2/g)	S_{DR} (CO_2) (m^2/g)	$V_{ultramicro}$[a] ($d < 0.7$ nm) ($cm^3\ g^{-1}$)	V_{micro}[b] ($d < 2$ nm) ($cm^3\ g^{-1}$)	V_{meso}[b] ($2 < d < 50$ nm) ($cm^3\ g^{-1}$)
A	1402	1283	0.49	0.53	0.17
A_{ox}	1382	1309	0.50	0.52	0.22
B	3487	1754	0.67	0.95	0.86
B_{ox}	3555	1597	0.61	0.97	0.89

(b)Oxygenated surface functionalities

	O_{1s} (at.%)	C–OR (286.3 ± 0.2 eV) (at.%)	C=O (287.5 ± 0.2 eV) (at.%)	–O–C=O (289.0 ± 0.2 eV) (at.%)
A	4.6	2.3	0.6	0.9
A_{ox}	14.8	4.3	2.3	4.2
B	5.0	1.6	0.9	1.3
B_{ox}	6.6	1.5	1.5	1.8

[a]Obtained after applying the Dubinin–Radushkevich equation to the CO_2 adsorption data.
[b]Obtained after applying the DFT method to the N_2 adsorption data.

with the increased amount of quinone-like (C=O in Table 1b) and pyrone-like functionalities (part of C=O and C–O in Table 1b) in A_{ox}. Due to this redox processes, the specific capacitance can be increased from 110 F g^{-1} to 214 F g^{-1} in acidic medium and from 124 F g^{-1} to 174 F g^{-1} in basic medium, when shifting from the pristine (A) to the oxidized sample (A_{ox}). Consequently, for the oxidized carbon, pseudo-faradaic redox reactions contribute in an important extent to the overall capacitance. According to Ref. [13], the smaller pseudo-faradaic contribution in alkaline solution would be most likely due to insufficiently available protons for the Q/HQ redox reaction. However, in alkaline electrolyte, there are other non-identified redox reactions involving oxygenated functionalities but giving less additional pseudo-capacitance than the Q/HQ pair.

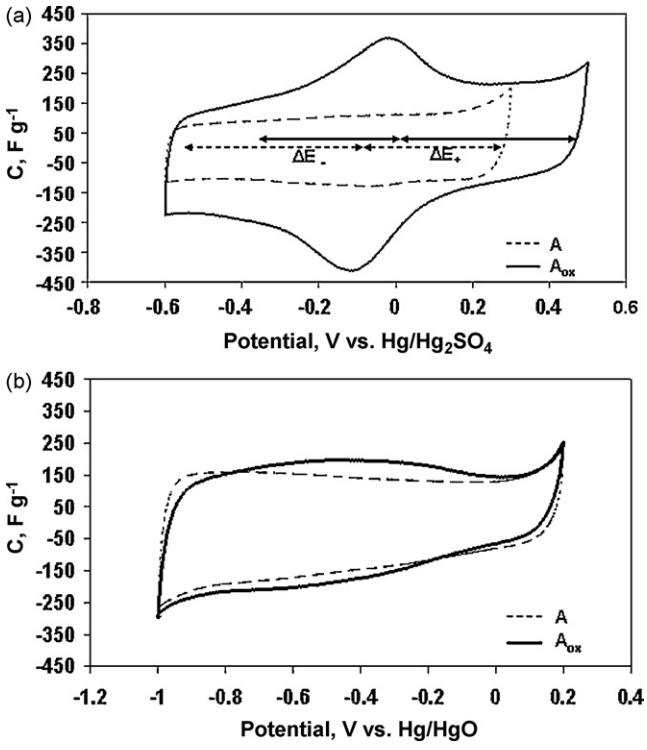

Fig. 1. Cyclic voltammograms of three-electrode cells with the activated carbons A and A_{ox} in (a) 1 mol L^{-1} H_2SO_4 (the arrows represent the values of the real ΔE for the positive and negative electrodes of a two-electrode cell charged up to 0.8 V) and (b) 6 mol L^{-1} KOH. Scan rate of potential 2 mV s^{-1}.

3.3. Symmetric systems

Fig. 2 shows that, when using a two-electrode cell in 1 mol L^{-1} H_2SO_4, the capacitance values of A and A_{ox} do not differ as much as in the three-electrode configuration (Fig. 1a); the capacitance increases only from 101 F g^{-1} to 137 F g^{-1} when shifting from A to A_{ox}. Such a result is not surprising, taking into account that a two-electrode cell is equivalent to two capacitors connected in series, with a capacitance (C) expressed by:

$$\frac{1}{C} = \frac{1}{C_1} + \frac{1}{C_2} \tag{3}$$

where C_1 and C_2 are the capacitance values for both electrodes; the capacitance of the device is essentially determined by the electrode with the smallest capacitance. Therefore a reference electrode has been introduced between the two AC electrodes in order to independently analyze their behavior during the charge/discharge of the capacitor, and especially to determine the capacitance and the real working potential range of each electrode. The dashed and solid arrows superimposed in Fig. 1a indicate the operating potential window (ΔE) of each electrode when a two-electrode configuration made of A and A_{ox}, respectively, is charged up to 0.8 V. It can be observed that the redox reactions involving the oxygenated functionalities influence simultaneously the equilibrium potential (EP) close to 0 V and the values of ΔE_+ and ΔE_- for the positive and negative electrodes when working in a symmetric two-electrode system. For the oxidized sample, the EP of the positive and negative electrodes is displaced to positive potentials, i.e. 0.013 V vs Hg/Hg_2SO_4. Consequently, the positive electrode of the symmetric capacitor based on A_{ox} works partly in the range where

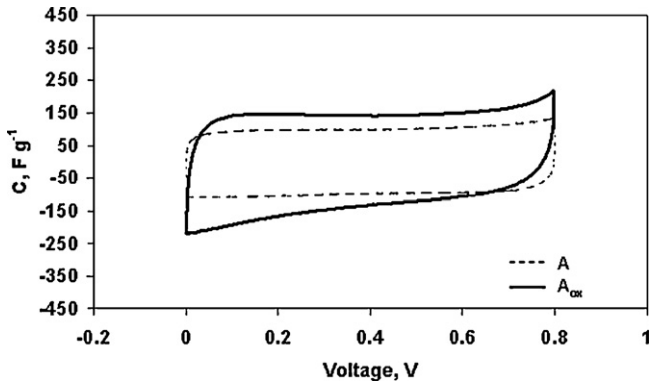

Fig. 2. Cyclic voltammograms of two-electrode cells with the carbons A and A_{ox} in 1 mol L^{-1} H_2SO_4. Scan rate of voltage 2 mV s^{-1}.

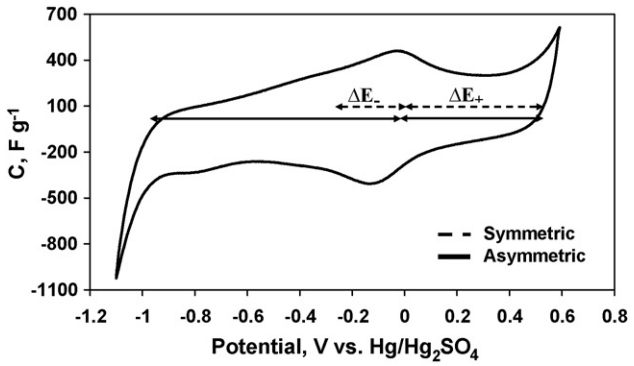

Fig. 3. Cyclic voltammogram of a three-electrode cell with A_{ox} in 1 mol L^{-1} H_2SO_4. Real ΔE values are included as arrows for the positive and negative electrodes when symmetric (dashed arrows) and asymmetric (continuous arrows) two-electrode cells are charged up to 0.8 V and 1.5 V, respectively. Scan rate of potential 2 mV s^{-1}.

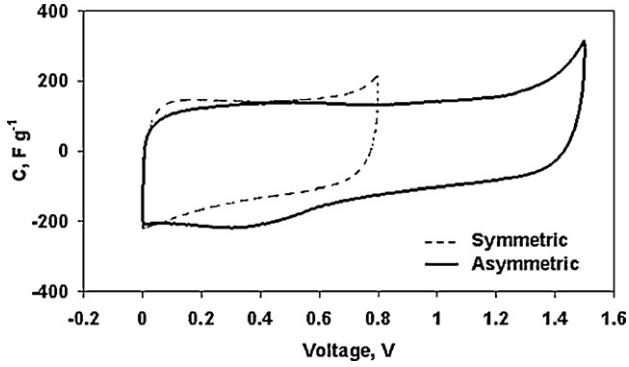

Fig. 4. Cyclic voltammograms of the symmetric and mass balanced asymmetric capacitors with the carbon A_{ox} in 1 mol L^{-1} H_2SO_4. Scan rate of voltage 2 mV s^{-1}.

redox reactions take place and only the capacitance of the negative electrode is enhanced after oxidation. The capacitance values are 105 F g^{-1} and 192 F g^{-1} for the positive and negative electrodes, respectively (see Table 2).

In conclusion, when pseudo-faradaic reactions contribute to the overall capacitance, it is crucial to take into account that they are potential dependent and that they consequently affect the performance of the positive and/or the negative electrode in a different way.

From the foregoing, the strategy to follow for improving the performance of a carbon/carbon capacitor consists in displacing the working potential range (ΔE) of the positive and negative electrodes in the potential range of the redox reactions. The shift to the desirable ΔE is possible by building asymmetric systems with a mass balance of positive and negative electrodes.

3.4. Asymmetric systems with mass balanced electrodes

At this point, one has to remind that, by principle, the charge (q) stored at the positive and negative electrodes is equivalent ($q_+ = q_-$). For each electrode, the charge stored depends on the specific capacitance (C), the potential range of the charge/discharge process (ΔE) and the mass of electrode (m) following Eq. (4):

$$q = C * \Delta E * m \quad (4)$$

Fig. 3 shows the CV of a three-electrode cell with A_{ox} in 1 mol L^{-1} H_2SO_4. The dashed arrows included in the figure represent the operating potential range of the two electrodes in a symmetric capacitor with two A_{ox} electrodes of similar mass, as discussed in the previous section. Since the redox reactions related with the oxygenated functionality take place mainly at the negative electrode, the capacitance value of the latter is higher than for the positive one. Then, taking into account that $q_+ = q_-$, it is found logically that $\Delta E_- < \Delta E_+$. In these conditions, if the cell voltage exceeds 0.8 V, the positive electrode reaches potential values corresponding to the irreversible oxidation of carbon. That means that the supercapacitor performance is limited by the positive electrode.

On the other hand, in an asymmetric configuration where the mass of the positive electrode (m_+) is twice the mass of the negative one (m_-), EP is slightly shifted by −23 mV (Fig. 3). If the cell is charged at a voltage higher than 0.8 V, the capacitance C_+ of the positive electrode increases (due to a higher participation of pseudo-faradaic reactions), while C_- of the negative one decreases (Table 2). Since $m_+ = 2m_-$, the principle of charge equivalence imposes that the negative electrode operates in a higher potential range than the positive one. However, Fig. 3 shows that the negative polarization of A_{ox} must be limited to −1.0 V vs Hg/Hg_2SO_4.

Fig. 4 displays the cyclic voltammograms obtained with symmetric and mass balanced asymmetric cells based on A_{ox} in 1 mol L^{-1} H_2SO_4. While the voltage must be limited to 0.8 V for the symmetric system, it can be increased up to 1.5 V without any electrolyte decomposition at the negative electrode or irreversible oxidation at the positive one for the asymmetric system. As a consequence, the energy density of the asymmetric configuration reaches 10.6 Wh kg^{-1} against only 3 Wh kg^{-1} in the symmetric one (Table 2). In addition, the cyclability of the asymmetric supercapacitor is excellent; after 1000 charge/discharge cycles at 1 A g^{-1} between 0 V and 1.5 V, the capacitance loss is only 5%, while it reaches 30% when cycling the symmetric system even at lower voltage (up to 0.8 V). The fact that the asymmetric configuration posses a good cyclability confirms the high reversibility of the redox reactions taking place between the oxygenated functionality and the electrolyte. Hence, the poor cycle life of the symmetric capacitor built with the same oxygen-rich electrode material is related with the operation of the positive electrode out of the stability potential window of the material and electrolyte.

Considering now 6 mol L^{-1} KOH as electrolyte, Fig. 1b shows that, with the activated carbon A, the redox reactions occur mainly in the negative range of potential. For a symmetric capacitor built with A, the EP is placed at −0.25 V vs Hg/HgO and the capacitance of the positive electrode is smaller than for the negative one (Table 2). In that case, applying a voltage higher than 0.6 V leads to

Table 2
Electrochemical characteristics of different symmetric and mass balanced asymmetric configurations.

AC	Cell configuration	Electrolyte	2-Electrodes			3-Electrodes			
			Cell voltage (V)	C (F g^{-1})	E (Wh kg^{-1})	EP[a] (V)	C_+[a] (F g^{-1})	C_-[a] (F g^{-1})	C[b] (F g^{-1})
A	Symmetric	H_2SO_4	0.8	101	2.2	−0.086	122	85	110
A_{ox}	Symmetric	H_2SO_4	0.8	137	3.0	0.013	105	192	214
A_{ox}	Asymmetric	H_2SO_4	1.5	136	10.6	−0.010	138	174	–
A	Symmetric	KOH	0.6	120	1.5	−0.250	98	149	124
A	Asymmetric	KOH	1.0	133	4.6	−0.380	109	171	–

[a] Values obtained by adding a reference electrode to the two-electrode cell.
[b] Classical three-electrode cell with a Pt counter electrode and a reference electrode.

the destructive oxidation of carbon at the positive electrode. In an asymmetric configuration with $m_+ = 2m_-$, EP is shifted of −13 mV; the capacitance of the positive electrode slightly increases and the cell voltage can reach 1.0 V because the operating potential range of the negative electrode can be enlarged. In consequence, even if the results are not as good as in acidic electrolyte, the energy density of the asymmetric configuration is 4.6 Wh kg^{-1} whereas only 1.5 Wh kg^{-1} were demonstrated for the symmetric configuration.

In conclusion, the performance of activated carbon-based supercapacitors in acidic or basic medium can be enhanced by simply balancing the mass of the electrodes. However, whatever the two-electrode configuration – either symmetric or mass balanced asymmetric – the redox reactions at the origin of pseudo-capacitive properties take place in only one electrode or partially in both electrodes, respectively. Due to the series dependence of capacitance (Eq. (3)), the electrode with the smallest capacitance determines the total cell capacitance, and a complete profit from the additional pseudo-faradaic reactions cannot be taken. Therefore, in order to optimize the activated carbon-based capacitors, we propose here a new asymmetric concept based on the use of two different carbons with a very marked pseudo-capacitive character.

3.5. Asymmetric systems with two different carbons adapted for positive and negative electrodes

Fig. 1a demonstrates that a highly oxidized carbon can be a good candidate for a positive electrode in 1 mol L^{-1} H_2SO_4, mainly for two reasons. Firstly, as it was discussed before, a pseudo-faradaic contribution is provided by the redox mechanisms involving the oxygenated functionalities. Secondly, by comparing the cyclic voltammograms of A and A_{ox}, it is easily seen that the positive limit of polarization, usually related with the destructive oxidation of carbon, is shifted to higher potential values for the A_{ox} carbon.

Now, the idea is to find for the negative electrode a carbon material with a high capacitance and a high negative limit of polarization. Fig. 5a shows the CVs for the two activated carbons, A and B, with different porous texture (Table 1a) and comparable oxygenated surface functionality (Table 1b). The highest capacitance is observed for B with the highest pore volume. Fig. 5a also presents the CV of B_{ox} obtained after a mild oxidation of carbon B. It results clearly that the slight increase of oxygenated functionalities by oxidation of B has a beneficial effect on the capacitive behavior and on the overpotential of hydrogen evolution. Actually, the integration of the CV for B_{ox} (Fig. 5a) provides capacitance values as high as 600 F g^{-1} for this carbon in 1 mol L^{-1} H_2SO_4.

Fig. 5b shows in detail the voltammograms of carbon B_{ox} obtained in 1 mol L^{-1} H_2SO_4 with different values of negative potential cut-off. When the potential cut-off is higher than the thermodynamic limit for dihydrogen evolution, e.g., −0.62 V vs Hg/Hg_2SO_4 at pH 0, the voltammograms are rectangular, typically for charging the electrical double-layer. As the potential cut-off is decreased to more negative values, nascent hydrogen starts to be produced by water electrodecomposition and to be immediately adsorbed in the carbon porosity; correspondingly, the hump growing ca. −0.5 V vs Hg/Hg_2SO_4 during the anodic scan characterizes the oxidation of hydrogen. This pseudo-faradaic contribution related with the reversible redox sorption of hydrogen in the pores is traduced in an additional capacitance. The presence of some oxygenated functionalities seems to be beneficial probably due to an enhancement of the carbon wettability. Also, and most important for our purpose, the overpotential for H_2 evolution is very high, allowing hydrogen to be sorbed in the porous carbon down to very low values of potential (−1.2 V vs Hg/Hg_2SO_4) without any gas evolution.

From the foregoing, two kinds of pseudo-faradaic properties of carbons, e.g., redox reactions with surface functional groups and

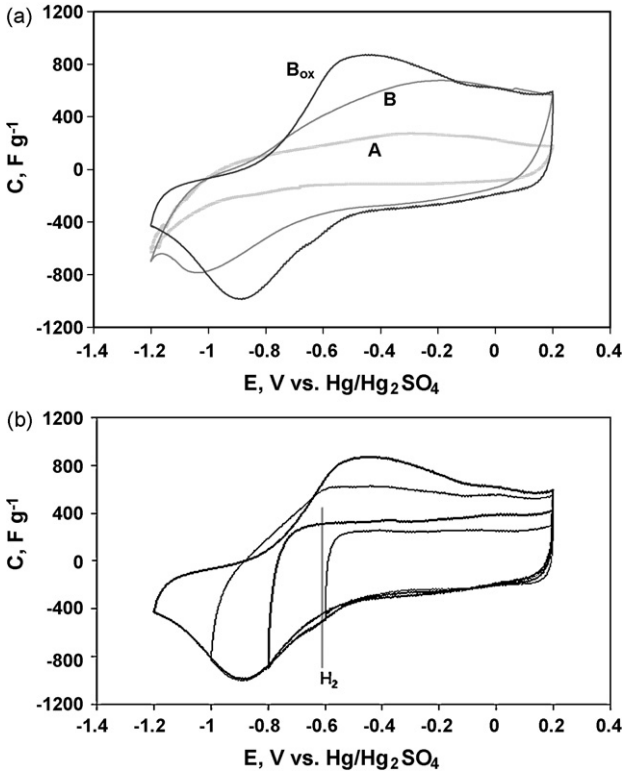

Fig. 5. Cyclic voltammograms of a three-electrode cell in 1 mol L^{-1} H_2SO_4 and with (a) the activated carbons A, B and B_{ox} in the negative range of potential and (b) the activated carbon B_{ox} at different values of negative potential cut-off. Scan rate of potential 2 mV s^{-1}.

reversible hydrogen storage, can be used in order to optimize the performance of the electrodes in different potential ranges. As example, Fig. 6 shows that the carbon A_{ox} operates in 1 mol L^{-1} H_2SO_4 with a relatively high capacitance at higher potential values than the carbon B_{ox}. Consequently, combining these two materials in an asymmetric cell with A_{ox} and B_{ox} at the positive and negative electrodes, respectively, should allow a voltage up to 1.8 V to be obtained without any destructive oxidation of the activated carbon A_{ox} or electrolyte decomposition.

In practice, for optimizing the performance of the two-electrode system, balancing the mass of electrodes is necessary in order to ensure them to operate in the highest range of potential. Fig. 7 shows the CV of an asymmetric capacitor where the mass of the negative and positive electrodes is 6.5 mg and 9 mg, respectively. This system can operate up to 1.6 V, against only 0.8 V for the sym-

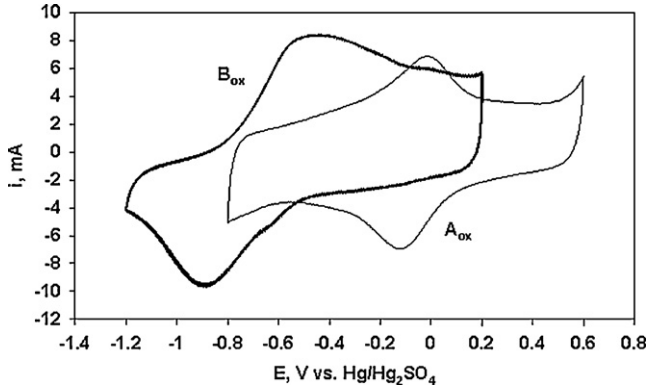

Fig. 6. Comparison of the cyclic voltammograms of three-electrode cells with the activated carbons A_{ox} and B_{ox} in 1 mol L^{-1} H_2SO_4. Scan rate of potential 2 mV s^{-1}.

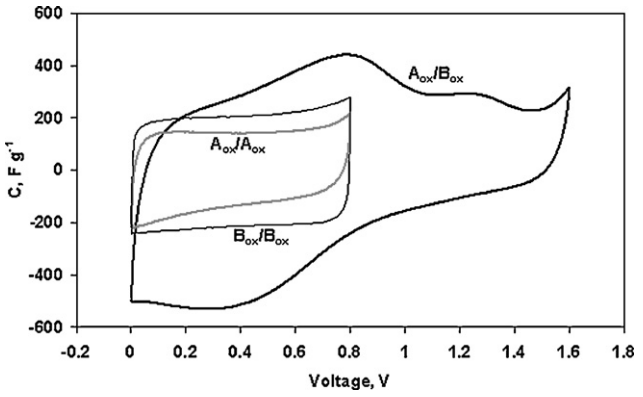

Fig. 7. Cyclic voltammograms of an optimized asymmetric A_{ox}/B_{ox} capacitor and of symmetric A_{ox}/A_{ox} and B_{ox}/B_{ox} capacitors in 1 mol L^{-1} H_2SO_4. Scan rate of voltage 2 mV s^{-1}.

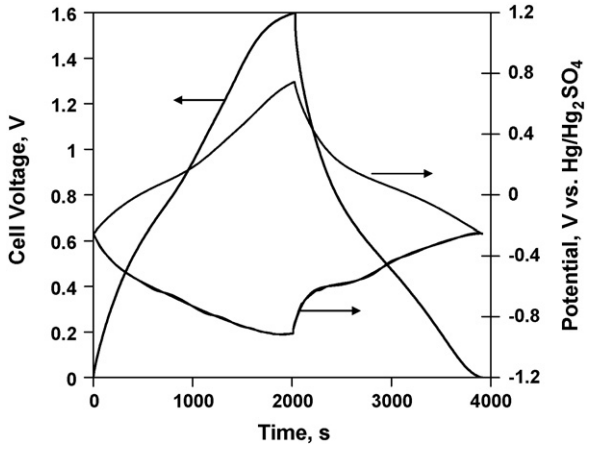

Fig. 8. Galvanostatic (I = 100 mA g^{-1}) charge–discharge profile of the asymmetric A_{ox}/B_{ox} capacitor in 1 mol L^{-1} H_2SO_4 and potential variation for the A_{ox} positive and B_{ox} negative electrodes adding a Hg/Hg_2SO_4 reference electrode in the cell.

metric A_{ox}/A_{ox} and B_{ox}/B_{ox} capacitors (Fig. 7). Due to the marked pseudo-faradaic character of the electrochemical processes at both electrodes, the shape of the CV for the asymmetric configuration is not perfectly rectangular. Fig. 8 shows the galvanostatic charge/discharge profile of the asymmetric two-electrode cell and the potential variation for the single electrodes when an Hg/Hg_2SO_4 reference electrode is added. The EP of the system is placed at −0.25 V vs Hg/Hg_2SO_4; when the cell is charged/discharged from 0 V to 1.6 V, the potential varies between −0.25 V and 0.73 V vs Hg/Hg_2SO_4 for the positive electrode and between −0.25 V and −0.87 V for the negative one. In such a situation, a close look at Fig. 6 reveals that the positive electrode fully operates in the potential window where redox reactions take place and a capacitance value of 230 F g^{-1} is obtained. According to Fig. 6, the negative electrode is also mainly operating where the redox reactions take place and the capacitance value of 474 F g^{-1} is close to the maximal possible (600 F g^{-1}) at electrode polarization down to −1.2 V.

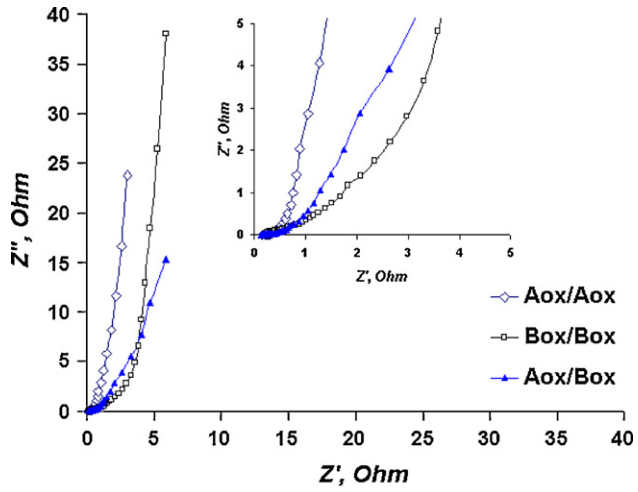

Fig. 9. Nyquist plots of the symmetric A_{ox}/A_{ox} and B_{ox}/B_{ox} capacitors and of the asymmetric A_{ox}/B_{ox} capacitor in 1 mol L^{-1} H_2SO_4 electrolyte.

Thus, due to the fact that each electrode operates almost within its optimal potential window, the capacitance of the non-symmetric configuration A_{ox}/B_{ox} reaches 321 F g^{-1}. This value is definitively higher than those obtained for the symmetric A_{ox}/A_{ox} and B_{ox}/B_{ox} configurations, e.g., 137 F g^{-1} and 230 F g^{-1}, respectively (Table 3).

Fig. 7 illustrates well that both capacitance and cell voltage are higher for the asymmetric than the symmetric systems. As a consequence, the maximum energy which can be extracted is close to 30 Wh kg^{-1}; it is 5–10 times higher than for symmetric capacitors working in the same electrolyte (Table 3). For comparison purposes, symmetric systems have been built using the most common organic electrolyte, i.e. 1 mol L^{-1} $TEABF_4$ in acetonitrile. The non-oxidized carbons were chosen as electrode materials, considering that in organic electrolytes the main mechanism is the formation of the electrical double-layer, which depends mainly on the porous texture. Moreover, the oxygenated surface functionalities would have a deleterious effect in enhancing the electrolyte decomposition [28]. The energy densities extracted from the A/A and B/B symmetric systems are 14.3 Wh kg^{-1} and 21.7 Wh kg^{-1}, respectively. Therefore, we can conclude that the energy density values of the asymmetric capacitor in H_2SO_4 and of the electrical double-layer capacitors in organic electrolyte are comparable.

The performances of the symmetric and asymmetric systems in aqueous H_2SO_4 were compared by impedance spectroscopy. Fig. 9 shows the Nyquist plots for the symmetric A_{ox}/A_{ox} and B_{ox}/B_{ox} cells and for the asymmetric A_{ox}/B_{ox} configuration. For the asymmetric capacitor, the phase angle is far from the 90° ideal value, demonstrating that the pseudo-faradaic reactions contribute more for this system than for the symmetric capacitors. In the case of the symmetric cells, the equivalent series resistance (ESR), extracted from the high frequency part of the plot (10 kHz), is smaller for the A_{ox}/A_{ox} system than the B_{ox}/B_{ox} one (Table 3). This result fits well with the higher porosity development and consequently lower conductivity of a capacitor based on the B_{ox} carbon in comparison to the A_{ox} one. When an asymmetric capacitor is assembled using these

Table 3
Comparative performance obtained from impedance spectroscopy and cyclic voltammetry experiments on the symmetric and asymmetric configurations of capacitors in 1 mol L^{-1} H_2SO_4.

Electrode material (+/−)	Cell configuration	Cell voltage (V)	C (F g^{-1})	E_{max}[a] (Wh kg^{-1})	ESR at 10 kHz (Ω)	P_{max}[a] (kW kg^{-1})
A_{ox}/A_{ox}	Symmetric	0.8	137	3.0	0.23	10.8
B_{ox}/B_{ox}	Symmetric	0.8	230	5.1	0.34	5.3
A_{ox}/B_{ox}	Asymmetric	1.6	321	28.6	0.26	37.5

[a] Specific energy and power calculated for the total mass of electrodes (including binding and conductivity agent).

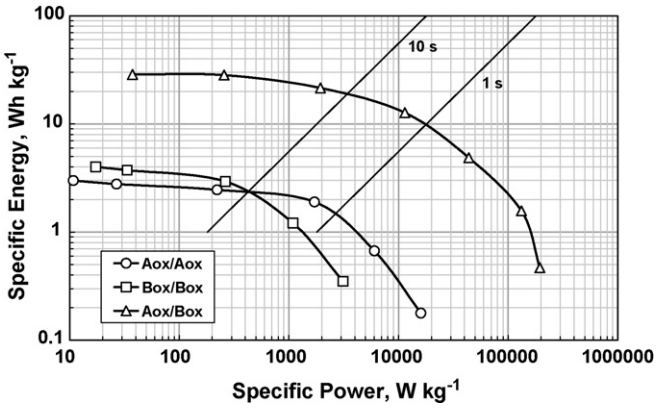

Fig. 10. Ragone plots for the asymmetric A_{ox}/B_{ox} capacitor at a voltage of 1.6 V (-△-) and for the A_{ox}/A_{ox} (-○-) and B_{ox}/B_{ox} (-□-) symmetric capacitors at a voltage of 0.8 V. Electrolyte: 1 mol L^{-1} H_2SO_4.

two carbons, the ESR is closer to the symmetric A_{ox}/A_{ox} system than to the B_{ox}/B_{ox} one (Table 3).

The ESR determined from the impedance spectroscopy measurements was used to calculate the maximum power according to relationship:

$$P_{max} = \frac{U_{max}^2}{4ESR * M} \quad (5)$$

where M is the total mass of both electrodes. Table 3 shows that the maximum power is much higher for the asymmetric capacitor than for any of the symmetric ones. The good performance of the asymmetric capacitor in terms of specific energy and power is highlighted by the Ragone plot presented in Fig. 10. At 10 s time constant, the A_{ox}/B_{ox} asymmetric capacitor largely outperforms both A_{ox}/A_{ox} and B_{ox}/B_{ox} symmetric capacitors.

Fig. 11 shows the cycle life of the asymmetric capacitor at a relatively high current density of 1 A g^{-1} for about 10,000 cycles. The small decrease (15%) of the discharge capacitance value observed during the first 2000 cycles is interpreted by a small evolution of the electrodes. After this conditioning period, the specific capacitance remains almost constant during the subsequent 8000 cycles, indicating a high stability of the supercapacitor during cycling. By contrast, the symmetric A_{ox}/A_{ox} system shows a dramatic decrease of capacitance during the first 1000 galvanostatic cycles, even at a low voltage of 0.8 V.

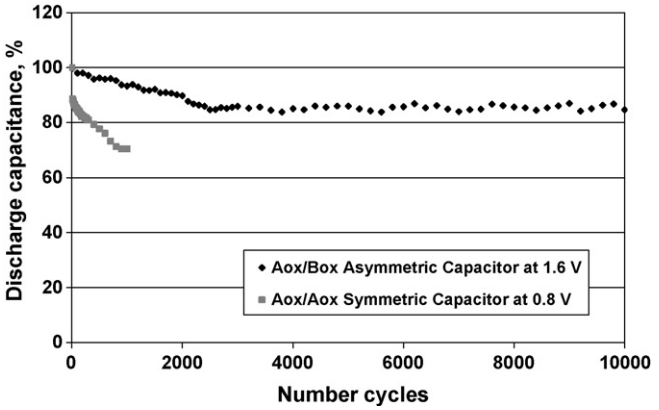

Fig. 11. Evolution of the specific discharge capacitance vs the number of cycles for the asymmetric A_{ox}/B_{ox} capacitor at 1.6 V and for the symmetric A_{ox}/A_{ox} one at 0.8 V in 1 mol L^{-1} H_2SO_4. Charge/discharge current 1 A g^{-1}.

4. Conclusion

A high energy density asymmetric electrochemical capacitor has been developed in aqueous electrolyte using only activated carbons (AC) as active electrode materials. Whereas charging the electrical double-layer is the only mechanism with activated carbons in organic electrolyte, an additional pseudo-faradaic redox contribution involving oxygenated functionalities plays an important role in aqueous medium. The redox reactions are potential dependent and affect the performance of the positive and/or negative electrode in a different way, depending on the electrolyte. Additionally, the oxygenated functionalities control the equilibrium potential (EP) and the potential window (ΔE) of the electrodes. By taking profit of such crucial effect of the oxygenated functionalities, we have shown that it is possible to improve the capacity and the operating voltage window of AC capacitors in aqueous medium either by balancing the mass of the electrodes or by using different optimized carbons as positive and negative electrode.

The potential window of each electrode could be adjusted by a mass balance of A_{ox} electrodes, allowing the cell voltage to be increased up to 1.5 V and an energy density of 10.6 Wh kg^{-1} to be obtained. However, the best results were obtained in the new concept of asymmetric capacitor consisting of two activated carbons adapted for the positive and negative electrodes. By an appropriate design of carbons, the potentials of H_2 evolution and destructive oxidation of activated carbon could be shifted to negative and positive potentials, respectively. Additionally, the capacitance of the system was enhanced due to the different pseudo-faradaic contributions at both electrodes. As a consequence, the electrochemical capacitor could be reversibly charged/discharged at 1.6 V with excellent cycle life. The power density, close to 40 kW kg^{-1} of carbon, is even higher than with any other available system in aqueous medium. The specific energy is about one order of magnitude higher than for symmetric carbon-based electrochemical capacitors in aqueous electrolyte, reaching closely the value of 30 Wh kg^{-1} which is comparable with the performance of EDLC in organic electrolyte.

Hence, the asymmetric system introduced here outperforms all existing electrochemical capacitors in aqueous electrolyte. It can be forecasted that safe and environment friendly devices of lower cost than EDLC in non-aqueous electrolyte could be fabricated by this technology.

References

[1] B.E. Conway, Electrochemical Supercapacitors, Kluwer Academic, Plenum Publishers, New York, 1999.
[2] E. Frackowiak, F. Béguin, Carbon 39 (2001) 937.
[3] V.V.N. Obreja, Physica E 40 (2008) 2596.
[4] J.P. Zheng, T.R. Jow, J. Electrochem. Soc. 142 (1995) L6.
[5] M. Toupin, T. Brousse, D. Bélanger, Chem. Mater. 14 (2002) 3946.
[6] E. Raymundo-Piñero, V. Khomenko, E. Frackowiak, F. Béguin, J. Electrochem. Soc. 152 (2005) A229.
[7] Y. Zhang, H. Feng, X. Wu, L. Wang, A. Zhang, T. Xia, H. Dong, X. Li, L. Zhang, Int. J. Hydrogen Energy 34 (2009) 4889.
[8] M. Mastragostino, C. Arbizzani, F. Soavi, Solid State Ionics 148 (2002) 493.
[9] V. Khomenko, E. Frackowiak, F. Béguin, Electrochim. Acta 50 (2005) 2499.
[10] C. Peng, S. Zhang, D. Jewell, G.Z. Chen, Prog. Nat. Sci. 18 (2008) 777.
[11] E. Frackowiak, G. Lota, J. Machnikowski, C. Vix-Guterl, F. Béguin, Electrochim. Acta 51 (2006) 2209.
[12] M. Seredych, D. Hulicova-Jurcakova, G.Q. Lu, T.J. Bandosz, Carbon 46 (2008) 1475.
[13] H.A. Andreas, B.E. Conway, Electrochim. Acta 51 (2006) 6510.
[14] H. Guo, Q. Gao, J. Power Sources 186 (2009) 551.
[15] E. Raymundo-Piñero, F. Leroux, F. Béguin, Adv. Mater. 18 (2006) 1877.
[16] G. Lota, K. Lota, E. Frackowiak, Electrochem. Commun. 9 (2007) 1828.
[17] L. Li, E. Liu, J. Li, Y. Yang, H. Shen, Z. Huang, X. Xiang, W. Li, J. Power Sources 195 (2009) 1516.
[18] K. Jurewicz, E. Frackowiak, F. Béguin, Appl. Phys. A 78 (2004) 981.
[19] F. Béguin, M. Friebe, K. Jurewicz, C. Vix-Guterl, J. Dentzer, E. Frackowiak, Carbon 44 (2006) 2392.
[20] J. Philips, D. Hewson, WO Patent 03/088374 A2 (2003).

[21] S. Razoumov, A. Klementov, S. Litvinenko, A. Beliakov, US Patent 6,222,723 B1 (2001).
[22] M.S. Hong, S.H. Lee, S.W. Kim, Electrochem. Solid State Lett. 5 (2002) A227.
[23] T. Brousse, M. Toupin, D. Bélanger, J. Electrochem. Soc. 151 (2004) A614.
[24] V. Khomenko, E. Raymundo-Piñero, F. Béguin, J. Power Sources 153 (2006) 183.
[25] M. Toupin, T. Brousse, D. Bélanger, Chem. Mater. 16 (2004) 3184.
[26] S. Biniak, A. Swiatkowski, M. Makula, in: L.R. Radovic (Ed.), Chemistry and Physics of Carbon, Marcel Dekker, New York, 2001, pp. 126–225.
[27] M.A. Montes-Moran, D. Suarez, J.A. Menendez, E. Fuente, Carbon 42 (2004) 1219.
[28] P. Azais, L. Duclaux, P. Florian, D. Massiot, M.A. Lillo-Rodenas, A. Linares-Solano, J.P. Peres, C. Jehoulet, F. Béguin, J. Power Sources 171 (2007) 1046.